Fermi National Accelerator Laboratory

FERMILAB-Pub-90/148-E
[E-711]

Average Fraction of Jet Momentum Carried by High $P_\perp$ Leading Hadrons*

G. Boca, D. Levinthal, F. Lopez, C. Georgiopoulos, H. Goldman, S. Hagopian, V. Hagopian, K. F. Johnson, J. Streets, K. Streets and H. B. White
Florida State University
Tallahassee, Florida 32306

M. Crisler, A. Lathrop and S. Pordes
Fermi National Accelerator Laboratory
P. O. Box 500
Batavia, Illinois 60510

M. Cummings and H. R. Gustafson
University of Michigan
Ann Arbor, Michigan 48109

July 1990

* Submitted to Z. Phys. C.

AVERAGE FRACTION

OF JET MOMENTUM CARRIED

BY HIGH $P_\perp$ LEADING HADRONS

G.Boca[a], D.Levinthal, F.Lopez[b], C.Georgiopoulos, H.Goldman
S.Hagopian, V.Hagopian, K.F.Johnson, J.Streets[d], K.Streets[c],H.B.White
Florida State University, Tallahassee, FL 32306

M.Crisler, A.Lathrop, S.Pordes.
Fermi National Accelerator Laboratory, Batavia, IL 60510

M.Cummings, H.R.Gustafson.
University of Michigan, Ann Arbor, MI 48109

[a] Now at University of Pavia, Sezione INFN, Pavia, Italy.
[b] Now at Argonne National Laboratory, Argonne, IL 60439.
[c] Now at University of Maryland, College Park, MD 20742.
[d] Now at Fermi National Accelerator Laboratory, Batavia, IL 60510

Abstract

The average fraction, $< z >$, of jet momentum carried by the leading charged hadron has been determined in the reaction $p + N \rightarrow h_1 + h_2 + X$ where N is the target nucleon; h_1, h_2 are the leading particles of two jets produced at high $P_\perp$. An 800 GeV/c proton beam and 4 nuclear targets: Be, Al, Fe and W were used. The $< z >$ distributions agree with the QCD-parton model predictions for single independent proton-nucleon scattering and independent fragmentation process.

Introduction

We present data taken at Fermilab between November 1987 and February 1988 in a fixed target experiment (E711) which was designed to measure the inclusive production of two back-to-back high $P_\perp$ charged hadrons at $\sqrt{s} = 38.8$ GeV . The reaction studied was

$$pN \rightarrow h_1 + h_2 + X$$

where p is the incoming 800 GeV/c proton, N the target nucleon, h_1 and h_2 are the outgoing hadrons in charged states $++$, $+-$, $--$, X is anything else produced in the reaction. Four types of target were used : beryllium, aluminium, iron and tungsten. The data come from an integrated luminosity per nucleon of 1.598×10^{37} cm^{-2} for Be, 6.090×10^{36} cm^{-2} for Al, 1.539×10^{37} cm^{-2} for Fe and 6.497×10^{36} cm^{-2} for W.

Experimentally it was found that at the present center of mass energy, when triggering on a high $P_\perp$ hadron, events are selected in which the high $P_\perp$ hadron is part of a jet[1][2]. The fraction of the trigger side momentum taken by the trigger particle ranges on average from 75 % to 90 %[1] (increasing with $x_\perp = 2P_\perp/\sqrt{s}$, the so called "trigger bias"[3]) and the direction of the trigger particle momentum is parallel (within $\pm 5°$ on average) to that of the jet[1]. This experiment triggered on two high $P_\perp$ hadrons with approximately equal and opposite transverse momenta, thus selecting jet events where the two scattered partons can be experimentally measured. This type of trigger brought the further advantage of discarding

events in which the colliding partons have a large intrinsic momentum (due to Fermi motion of the partons inside nucleons[4]).

In this article we present a measurement of $< z >$, the average fraction of energy of the high $P_\perp$ jet carried by the high $P_\perp$ hadron ("leading hadron") :

$$< z >\equiv \left\langle \frac{E_{leading}}{E_{jet}} \right\rangle$$

In the QCD[5] theoretical framework, the fragmentation variable $< z >$ is related, for high $P_\perp$ particles, to the distribution functions of the colliding hadrons, to the parton-parton scattering cross section and to the fragmentation functions of the scattered partons. The QCD-parton model can successfully describe a wide range of processes at different energies such as e^+e^-, pp, $p\bar{p}$ reactions in collider machines[6]. Whether high $P_\perp$ phenomena can be described by functions independent of the rest of the surrounding environment when using nuclear targets is still an open question. An answer will be given by comparing plots of $< z >$ calculated from data produced with nuclear targets with the QCD predictions valid for isolated particle-particle scattering.

Experimental Details

The apparatus (Figure 1), a double arm spectrometer, triggered calorimetrically and with a high resolution magnetic momentum measurement, has been described extensively elsewhere[7]. Here a short description is

presented. The detector was designed to have a large acceptance for all charge states in both the polar angle defined in the rest frame of the di-hadron state ($|cos\theta^*|$) < 0.5), and in the central rapidity region in the proton-nucleon center of mass ($|Y_{pN}| < 0.5$). A 1 mm 10% interaction length target (beryllium, aluminium, iron, tungsten) was placed just upstream of two large aperture analysis magnets, which provided a momentum kick of 1.16 GeV/c in the horizontal plane. Downstream of the magnets there were 5 stations of wire chambers (4 views per station) to reconstruct the particle tracks, four planes of hodoscopes and two calorimeters used for triggering. The sampling calorimeters were comprised each of 16 horizontal segments and covered the azimuthal range $\pm 25°$ about the vertical. They were divided in four longitudinal sections. The first had lead as absorber and served to identify electromagnetic showers (29.7 radiation lengths). The other three sections had iron as absorber and identified the hadronic showers, contained at a 99% level in the whole calorimeter. The apparatus was designed to accept a beam intensity of 10^8 protons per second. To avoid any sensitivity to the beam and other particles in the median plane, it was made insensitive to radiation within ± 20 mrad of the beam axis in the vertical direction. To accomplish this, the wire chambers were deadened across a central horizontal band and the calorimeters and hodoscopes were positioned above and below the beam axis in the vertical direction.

The experiment trigger was provided by the calorimeters and required a localized energy deposition in each calorimeter with a transverse energy

greater than 2 GeV, and a total transverse energy greater than 6 GeV. The trigger selected charged hadrons by requiring signals from the hodoscopes in front of the energy clusters.

Triggering on scatters in the vertical plane and measuring momenta by bending in the horizontal plane minimized the effect of the magnetic bending on the trigger. This allowed the use of a high magnetic field and a long lever arm, thus improving the track momentum resolution. To allow the experiment to operate at high rates, a narrow target was used, thus defining the production vertex and eliminating the need for track measurements upstream of the magnet, where the particle flux density was highest. The wire chambers were designed to operate with small collection times and equipped with pre-amplifiers to reduce the operating gain required. The hodoscopes and calorimeters were constructed with fast scintillator and photomuliplier tubes and low dispersion cables to avoid pile-up effects.

Analysis and cuts

Charged tracks were reconstructed, using the wire chamber information, by an algorithm[8] written in vectorized code. The particle momenta are calculated from the downstream trajectory assuming that the interaction occurred at the center of the target. The uncertainty in the momentum is due to the size of the target and the chamber resolution. Above $p =$

20 GeV/c the momentum resolution is dominated by the target width, and can be expressed as $\delta p/p = kp$, where k takes a value between 2.5×10^{-4} and 2.8×10^{-4} $(\mathrm{GeV/c})^{-1}$ for the four targets. The resolution function was also calculated by superimposing montecarlo tracks onto data events and comparing the momentum of the generated track with that found by the tracking algorithm. This technique gave a result in agreement with the direct calculation. The high $P_\perp$ di-hadron events were selected from the initial data sample by requiring:

(a) a loose cut on the vertical (non-bend view) position of the tracks at the target;

(b) the requirement that the di-hadron alone satisfied the trigger and

(c) consistency between the track momentum and the associated calorimeter energy.

The fiducial volume was restricted in the calorimeter to ensure shower containment. The lower di-hadron mass limit of 6 $\mathrm{GeV/c^2}$ was determined from the measurement of the efficiency of the hardware trigger. This efficiency was found to be independent of target type.

Two backgrounds which could have simulated a di-hadron event have been considered. The first is from proton interactions in material other than the target, the second from coincidental hadrons from two proton interaction within the trigger gate. Several runs were taken with the target removed and the data were analyzed in exactly the same method

as the target data. Normalizing the number of events found by the beam flux, the fraction of this background in the data samples were found to be 2.7% for Be, 1.4% for Al, 1.2% for Fe and 1.0% for W. Both calculation and measurement of uncorrelated hadrons shows the latter background to be negligible ($< 1\%$).

In determining $< Z >$ the leading hadron of the two high $P_\perp$ jets, one above and one below the beam axis, were identified among the charged hadrons satisfying the cuts (a), (b) and (c). If more than one charged track hitting the same calorimeter passed these cuts, the one with the highest momentum was chosen. The energy of the leading hadron, $E_{leading}$ was assumed equal to its momentum measured by the chambers. The energy of the jet, E_{jet}, was determined by also including the calorimeter information. The jet spray particles were defined as those lying inside a 'jet cone' around the leading hadron direction, assumed to be the same as the jet direction. The jet cone angular aperture, Θ_{cone} in the di-hadron center of mass frame, was chosen considering the histogram of $\cos\theta_{soft}$, where θ_{soft} is the angle, in the di-hadron center of mass, between the leading hadron and all the other softer charged particles (figure 2, dashed line). The sharp peak near to $\theta_{soft} = 0$ indicates the presence of jet structure in the data. To prove this was not simply an acceptance effect, the same histogram is plotted (figure 2, solid line) substituting, for each event, the leading hadron momenta with the ones of the previous selected event. The histogram broadens considerably and the sharp peak disappears. The value of $\Theta_{cone} = 21.6°$ ($\cos\Theta_{cone} = 0.92$) was chosen.

The total energy of the jet is given by

$$E_{jet} \equiv E_{leading} + E_{non-leading}$$

where $E_{non-leading}$ is the energy of the soft particles lying in the jet cone. $E_{non-leading}$ was calculated assuming

$$E_{non-leading} = kE_{\gamma}$$

were E_{γ} is the energy of the γ's inside the jet cone. These γ's were produced from the electromagnetic decay of neutral hadrons (mainly π^{o}'s) belonging to the jet spray. If the jet non-leading particles were all π's, the constant k would be equal to 3 from isospin symmetry considerations[2]. The determination of k was achieved by running a LUND montecarlo[9], which simulated two high $P_{\perp}$ jet events which were then passed through the analysis cut chain. The values of k, calculated for different ranges of $P_{\perp}$ and $\cos\theta^{\star}$ of the leading hadrons are listed in table 1.

The value of E_{γ} was obtained measuring the energy deposition in that portion of the calorimeter intersected by the jet cone, projected from the target to the calorimeter front face. Only the energy deposited in the first longitudinal section of the calorimeter (the electromagnetic one) was taken into account. Jets whose cone was not completely contained in calorimeter active region were rejected. The virtues of considering only the jet γ energy are apparent : first of all the γ's, not affected by the magnets, could reach the active part of the calorimeters, secondly the contamination of E_{γ} due to the few soft charged hadrons reaching the calorimeter was small also because they essentially did not shower in the

electromagnetic section of the calorimeter. The contamination caused by the small deposition of energy by the leading hadron in that portion of the electromagnetic section of the calorimeter intersected by the jet cone, was calculated with a montecarlo[10] which simulated the average energy deposited as a function of the leading hadron initial energy. E_γ was then corrected on a jet by jet basis (the correction was 3% on average) and the error introduced in the calculation of $< \mathcal{Z} >$ by considering average corrections to E_γ was included in the computation of the systematic error.

Two other corrections were applied to the data. The first took into account the possible underestimation of the neutral energy of a jet due to the definition of the jet cone aperture angle of 21.6°. A LUND montecarlo was used to calculate average corrections (function of $P_\perp$ and $\cos\theta^\star$ of the leading hadron) which were applied to the data for each jet. These corrections were always smaller than 20% of the neutral energy value and were 15% on average. They are listed in table 2. The second correction took into account the absorption of the γ's of the jet neutral energy in the target. A montecarlo generated γ's in the target uniformly, pointing to the calorimeter, and calculated the average fraction of energy reaching the calorimeter. This fraction was essentially independent of the initial γ energy in the range from 1 to 500 GeV.

Results

Different target comparison

We noticed that all the data plots presented no significant statistical differences for different target types. An instance of this is shown in figure 3, where $< \mathcal{Z} >$ is plotted versus $\cos\theta^{\star}$, scattering angle of the leading hadron in the di-hadron center of mass, for the different targets. The quantity $< \mathcal{Z} >$ is calculated when the jets have their cone completely included in the active calorimeter region (the "single jet" plots) and when both jets of an event satisfied this cut ("two jet" plots). The independence on the targets is in agreement with the results of our A-dependence measurement ($\alpha = 1.043 \pm 0.011 \pm 0.025$) of the high $P_{\perp}$ event production cross section reported recently[7][15].

Comparison between data and QCD-parton model predictions

In the following plots the data are shown for all the targets together. The quantity $< \mathcal{Z} >$ is plotted as a function of $P_{\perp}$, transverse momentum of the leading hadron, (figures 4 through 6), $\cos\theta^{\star}$ (figures 7 through 9), and versus $\cos\theta^{\star}$ in selected bins of mass of the di-hadron system (figures 10 through 15). The data shown are "single jet" and "two jet" events when the leading hadron has positive charge, negative charge and either charge. In all the figures black circles represent the data, while open triangles show the theoretical predictions. Statistical and systematic errors

are shown in the data. The theoretical predictions are calculated using a QCD-parton model montecarlo, for the same $P_\perp$ and $\cos\theta^\star$ intervals. They were calculated with an independent fragmentation mechanism, and assuming a proton colliding with an isolated nucleon. The parton-parton scattering matrix was calculated in the leading logarithmic approximation assuming for α_s four quark flavours. The structure functions used were the Duke and Owens set 1[11], evolved according to the Altarelli-Parisi equations[12]. The fragmentation functions were determined from recently published data[13] and evolved according to Umematsu and Owens[14]. In the leading logarithmic approximation the characteristic scale variable and scale parameter can be chosen to be the same for the evolved structure functions, fragmentation functions and for α_s[6]. Here $Q^2 \equiv P_\perp^2$ and $\Lambda = 200$ MeV/c were chosen. The montecarlo technique allowed the use of non-collinear kinematics for the colliding parton and the leading hadron product of the fragmenting parton. The average transverse momentum used were 700 MeV/c and 300 MeV/c respectively. The montecarlo generated events were then selected by simulating the acceptance of the apparatus. The errors shown on the theoretical predictions are purely statistical.

No statistically significant difference is observed between corresponding plots for different charges of the leading hadron. In general the theoretical distributions agree well with the data. This is especially true for $< \mathcal{Z} >$ plotted as a function of the leading hadron $P_\perp$ ranges. The discrepancies between data and theory in the $< \mathcal{Z} >$ versus $\cos\theta^\star$ plots can

be explained with the low statistics populating the extreme bins especially when increasingly higher di-hadron mass slices are selected.

Conclusions

From inspection of the experimental plots one can conclude that within experimental errors :

1) at $\sqrt{s} = 38.8$ GeV the parton high $P_\perp$ scattering and fragmentation is not affected by interactions taking place at the nuclear level

2) at this energy the QCD-parton model with independent fragmentation describes well the experimental data

3) if we assume that, given their large average value of $\mathcal{Z}$, the leading hadron have the same charge as the outgoing parton it originates from, the fragmentation seems to be independent from the flavour of the parton, as shown by the absence of any significant difference of $< \mathcal{Z} >$ for different charges of the leading hadron.

We should like to thank the American National Science Foundation and the U.S. Department of Energy for funding this work. The experiment would not have been possible without the fine technical support of Fermilab and Florida State University. We should like to thank the following who took part in the construction and early test run : M.Bertoldi,

T.Kramer and S.Ploplys. Finally a very special thank to Prof. S.Ratti of Pavia University for his precious suggestions and supervision during the analysis.

TABLE 1

Results of the montecarlo calculating the factor k relating the jet neutral energy and its total 'soft' energy, for different leading hadron $P_\perp$ and $\cos\theta^\star$ ranges.

Leading hadron $P_\perp$ range (GeV/c)	k
2.5 - 3.5	3.060
3.5 - 4.5	3.006
4.5 - 5.5	3.121
5.5 - 6.5	3.001
6.5 - 7.5	3.000

Leading hadron $\cos\theta^\star$ range	k
-0.6 / -0.4	3.000
-0.4 / -0.2	3.050
-0.2 / 0.	3.130
0. / 0.2	3.151
0.2 / 0.4	3.162
0.4 / 0.6	3.000

TABLE 2

Percentage correction of the jet neutral energy, for different leading hadron $P_\perp$ and $\cos\theta^*$ ranges, due to the choice of $\cos\Theta_{cone} = 0.92$

Leading hadron $P_\perp$ range (GeV/c)	correction (%)
2.5 - 3.5	10
3.5 - 4.5	17
4.5 - 5.5	12
5.5 - 6.5	21
6.5 - 7.5	18

Leading hadron $\cos\theta^*$ range	correction (%)
-0.6 / -0.4	12
-0.4 / -0.2	13
-0.2 / 0.	16
0. / 0.2	16
0.2 / 0.4	15
0.4 / 0.6	11

References

[1] A.L.S. Angelis *et al.*, Nuclear Phys. **B209** 284 (1982)

[2] A.L.S. Angelis *et al.*, Phys. Scripta **19** 116 (1979)

[3] M.Jacob, P.Landshoff, Phys. Reports **48 C** 286 (1978)

[4] J.Owens, Phys. Rev. **D 20** 221 (1979)

R.Baier, J.Engels and B.Petersson, Z. Phys. **C 2** 265 (1979).

J.Gunion and B.Petersson, Phys. Rev. **D 22** 629 (1980).

[5] S.Berman, J.Bjorken, J.Kogut, Phys. Rev. **D4** 3388 (1971).

B.L.Combridge, J.Kripfganz, J.Ranft, Phys.Lett. **70B** 234 (1977).

[6] J.F. Owens, Rev. Mod. Phys. **59** 465 (1987)

[7] K.Streets, Ph.D. Dissertation. Florida State University (1989).

[8] C.Georgiopoulos, J.H.Goldman, M.Hodus, NIM **A261** 493 (1987)

[9] The Lund montecarlo programs, CERN long writeup, 3 April 1987.

[10] GEANT3 manual, CERN Data Handling Division, DD/EE/84-1 (1987).

[11] D.W. Duke and J.F.Owens, Phys. Rev. **D 30** 49 (1984)

[12] G.Altarelli and G.Parisi, Nucl. Phys. **B126** 298 (1977)

[13] EMC collaboration, CERN-EP/89-25 January 31, 1989

[14] T.Umematsu, Phys. Lett. **79B** 97 (1978)

J.F.Owens, Phys. Lett. **76B** 85 (1978)

[15] K.Streets *et al.*, Fermilab preprint Pub-89/42-E, February 1989

Figure Captions

Figure 1

Plan view of the apparatus.

Figure 2

Plot of the angle θ_{soft}, in the di-hadron center of mass, between the leading hadron and the other 'soft' charged particles (dotted line). Also shown is the θ_{soft} angle when the leading hadron momenta are substituted by the ones of the previous selected event (solid line).

Figure 3

$< z >$, function of $\cos\theta^*$ for different targets, single jet events and two jet events.

Figure 4

$< z >$, function of $P_\perp$ of the leading hadron for single and two jet events and both leading hadron charges.

- • experimental data
- △ theoretical predictions

Figure 5

$< \mathcal{Z} >$, function of $P_\perp$ of the leading hadron for single and two jet events and positive leading hadron charge.

- • experimental data
- △ theoretical predictions

Figure 6

$< \mathcal{Z} >$, function of $P_\perp$ of the leading hadron for single and two jet events and negative leading hadron charge.

- • experimental data
- △ theoretical predictions

Figure 7

$< \mathcal{Z} >$, function of $\cos\theta^\star$ of the leading hadron for single and two jet events and both leading hadron charges.

- • experimental data
- △ theoretical predictions

Figure 8

$< \mathcal{Z} >$, function of $\cos\theta^\star$ of the leading hadron for single and two jet events and positive leading hadron charge.

- • experimental data

△ theoretical predictions

Figure 9

$< z >$, function of $\cos\theta^{\star}$ of the leading hadron for single and two jet events and negative leading hadron charge.

• experimental data

△ theoretical predictions

Figure 10

$< z >$, function of $\cos\theta^{\star}$ of the leading hadron for single and two jet events, for different $M_{di-hadron}$ slices and both leading hadron charges.

• experimental data

△ theoretical predictions

Figure 11

$< z >$, function of $\cos\theta^{\star}$ of the leading hadron for single and two jet events, for different $M_{di-hadron}$ slices and both leading hadron charges.

• experimental data

△ theoretical predictions

Figure 12

$< z >$, function of $\cos\theta^*$ of the leading hadron for single and two jet events, for different $M_{di-hadron}$ slices and positive leading hadron charge.

- • experimental data
- △ theoretical predictions

Figure 13

$< z >$, function of $\cos\theta^*$ of the leading hadron for single and two jet events, for different $M_{di-hadron}$ slices and positive leading hadron charge.

- • experimental data
- △ theoretical predictions

Figure 14

$< z >$, function of $\cos\theta^*$ of the leading hadron for single and two jet events, for different $M_{di-hadron}$ slices and negative leading hadron charge.

- • experimental data
- △ theoretical predictions

Figure 15

$< z >$, function of $\cos\theta^*$ of the leading hadron for single and two jet events, for different $M_{di-hadron}$ slices and negative leading hadron charge.

- • experimental data
- △ theoretical predictions

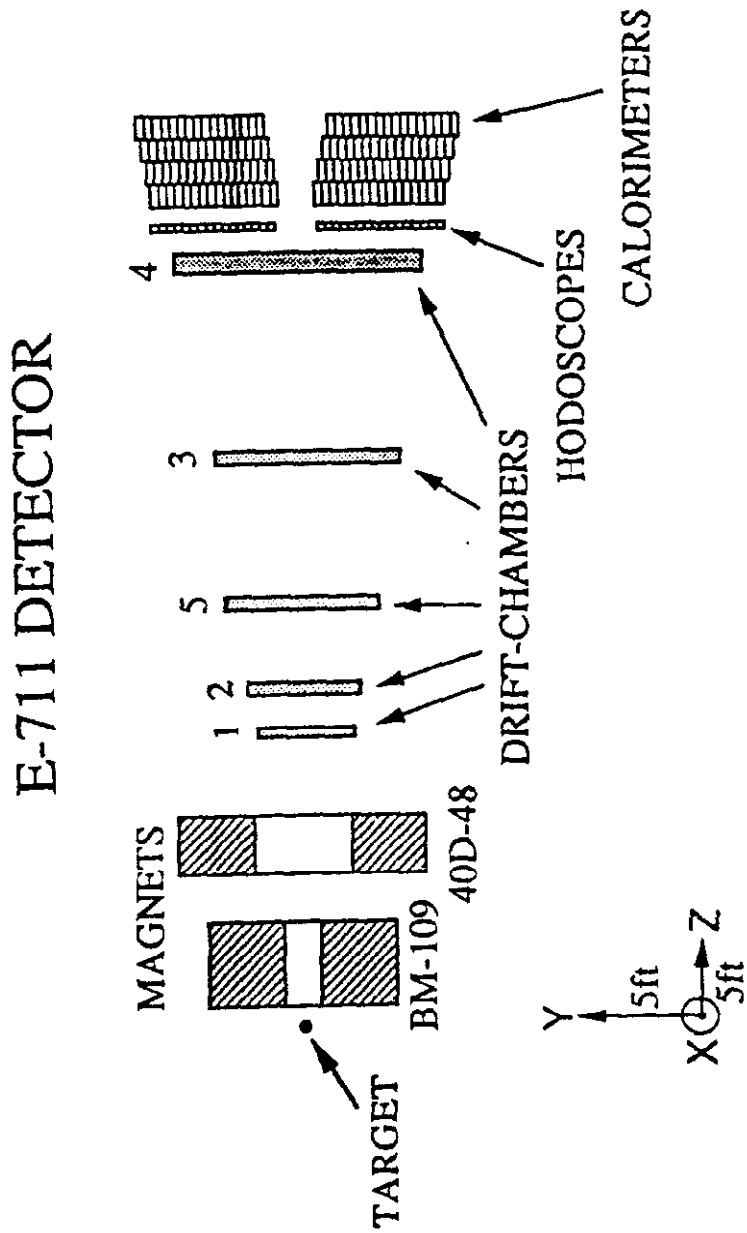

Plan view of the apparatus.

Figure 1

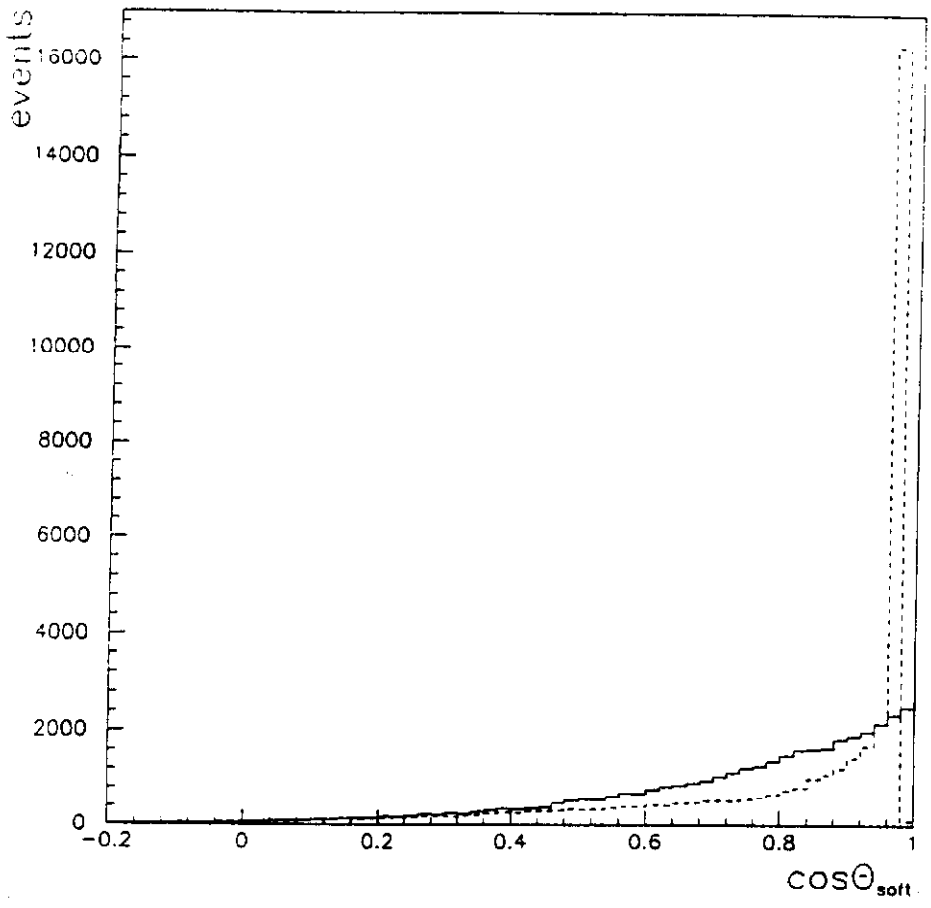

Plot of the angle θ_{soft}, in the di-hadron center of mass, between the leading hadron and the other 'soft' charged particles (dotted line). Also shown is the θ_{soft} angle when the leading hadron momenta are substituted by the ones of the previous selected event (solid line).

Figure 2

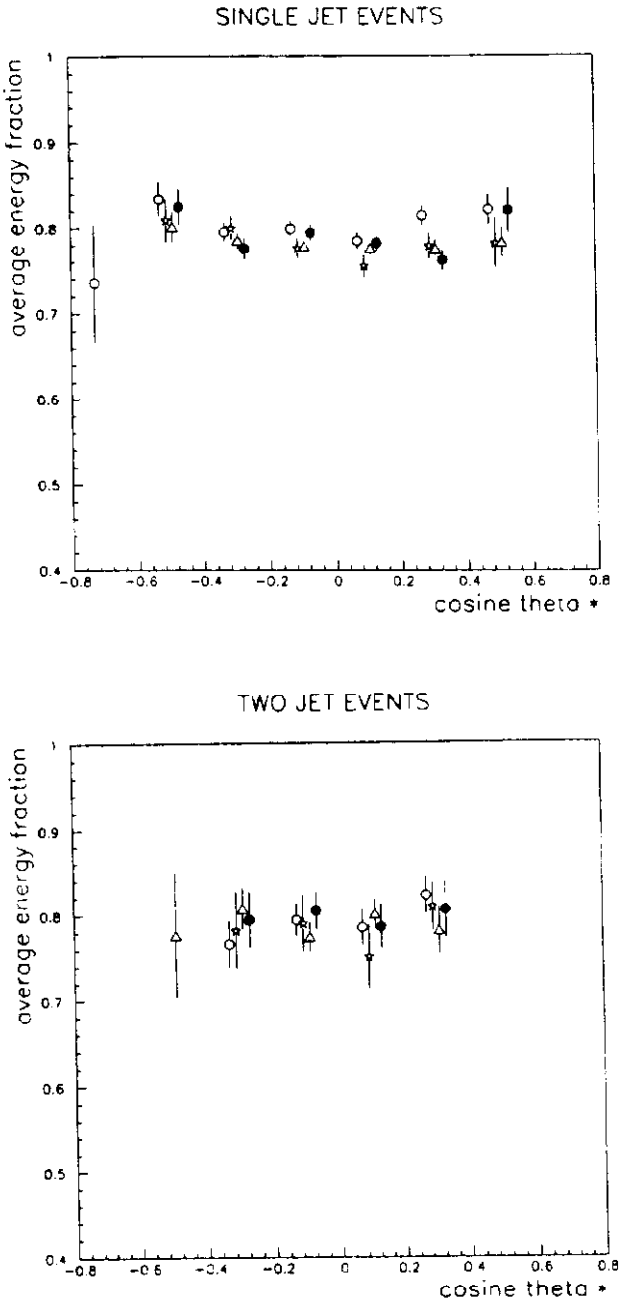

$< \mathcal{Z} >$, function of $\cos\theta^{\star}$ for different targets, single jet events and two jet events.

o Be target

$\star$ Al target

$\triangle$ Fe target

• W target

Figure 3

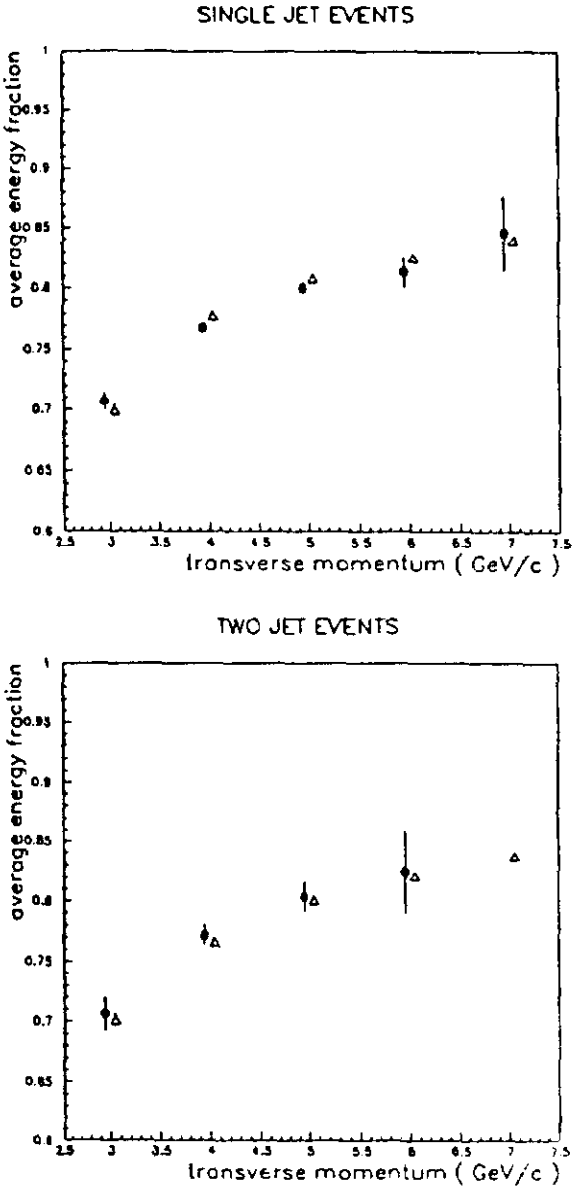

$< z >$, function of $P_\perp$ of the leading hadron for single and two jet events and both leading hadron charges.

- • experimental data
- △ theoretical predictions

Figure 4

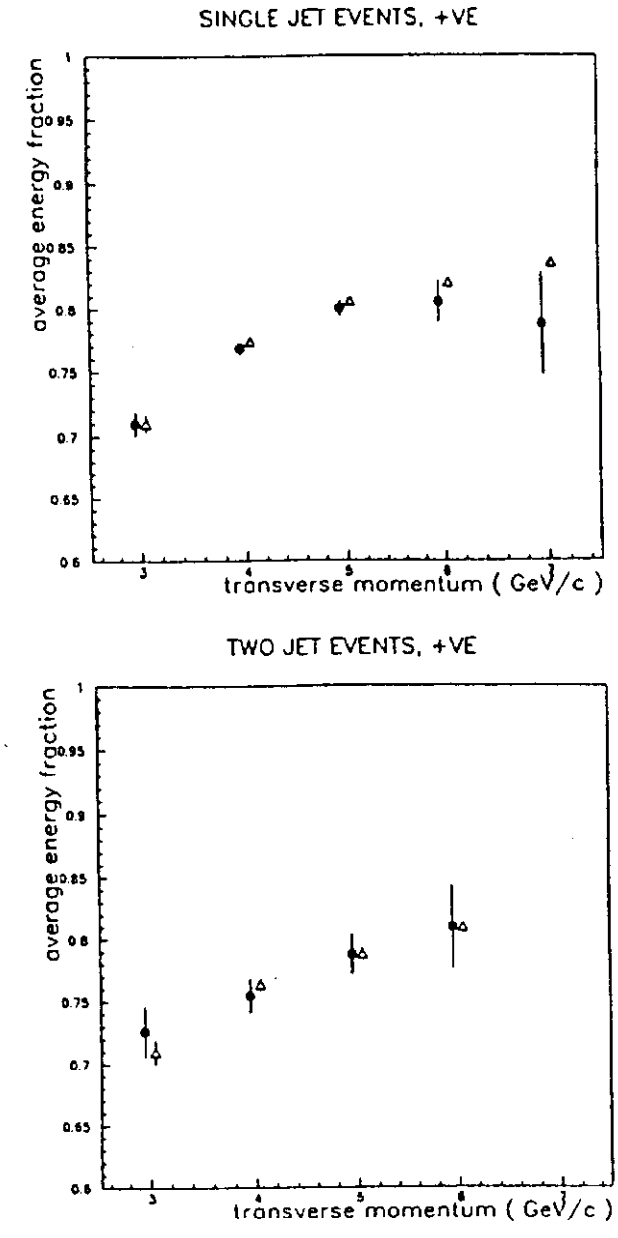

$< \mathcal{Z} >$, function of $P_\perp$ of the leading hadron for single and two jet events and positive leading hadron charge.

- • experimental data
- △ theoretical predictions

Figure 5

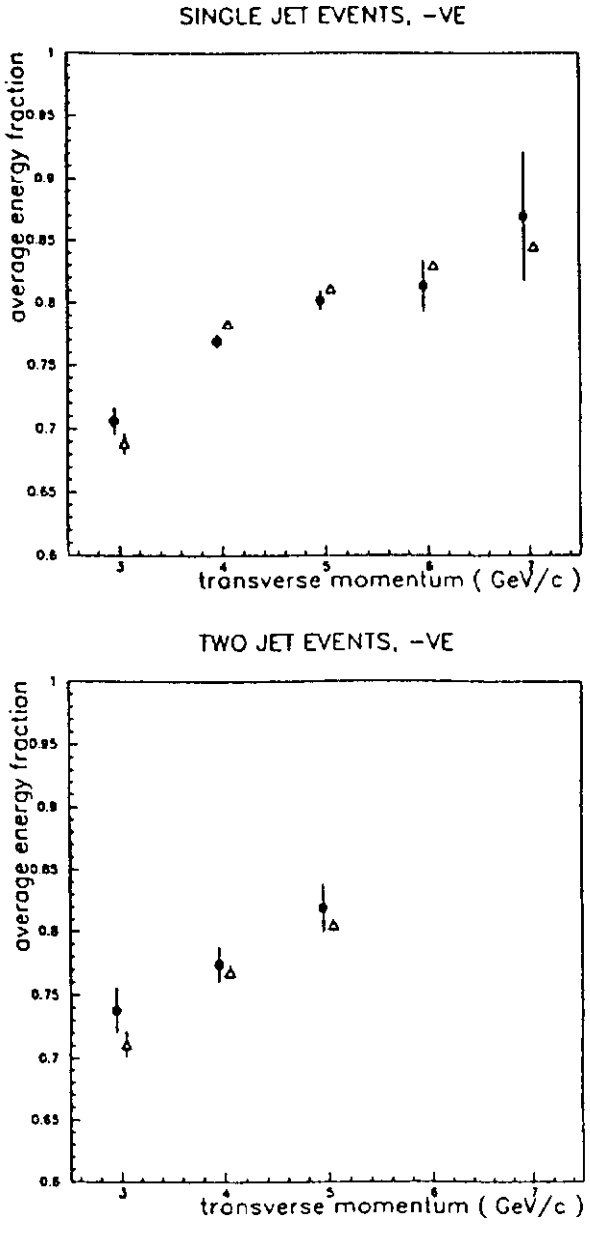

$< z >$, function of $P_\perp$ of the leading hadron for single and two jet events and negative leading hadron charge.

- • experimental data
- △ theoretical predictions

Figure 6

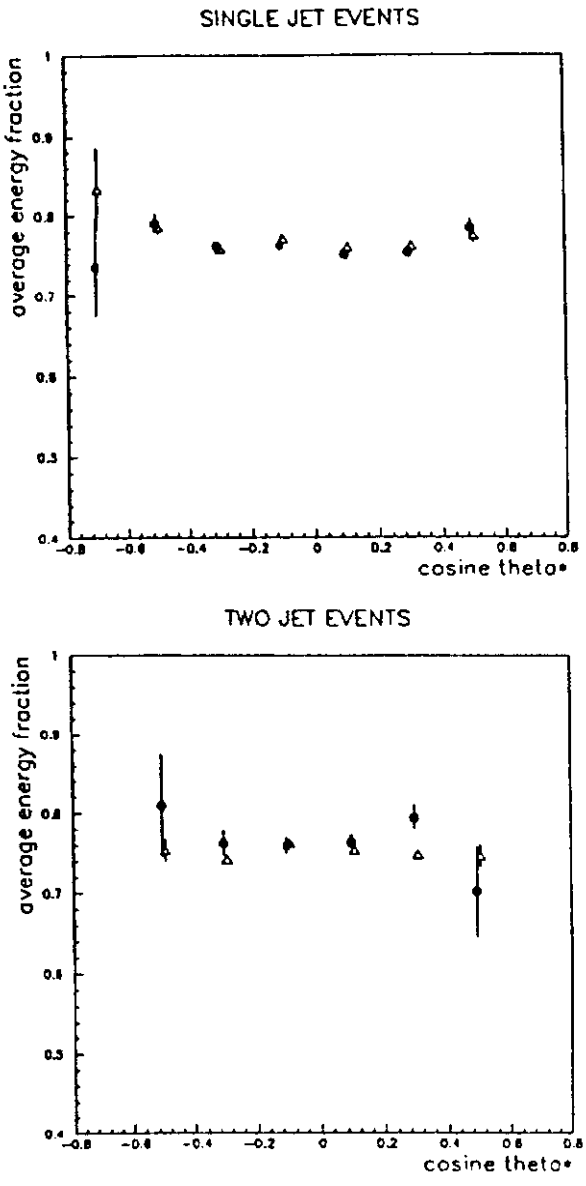

$< \mathcal{Z} >$, function of $\cos\theta^{\star}$ of the leading hadron for single and two jet events and both leading hadron charges.

- • experimental data
- △ theoretical predictions

Figure 7

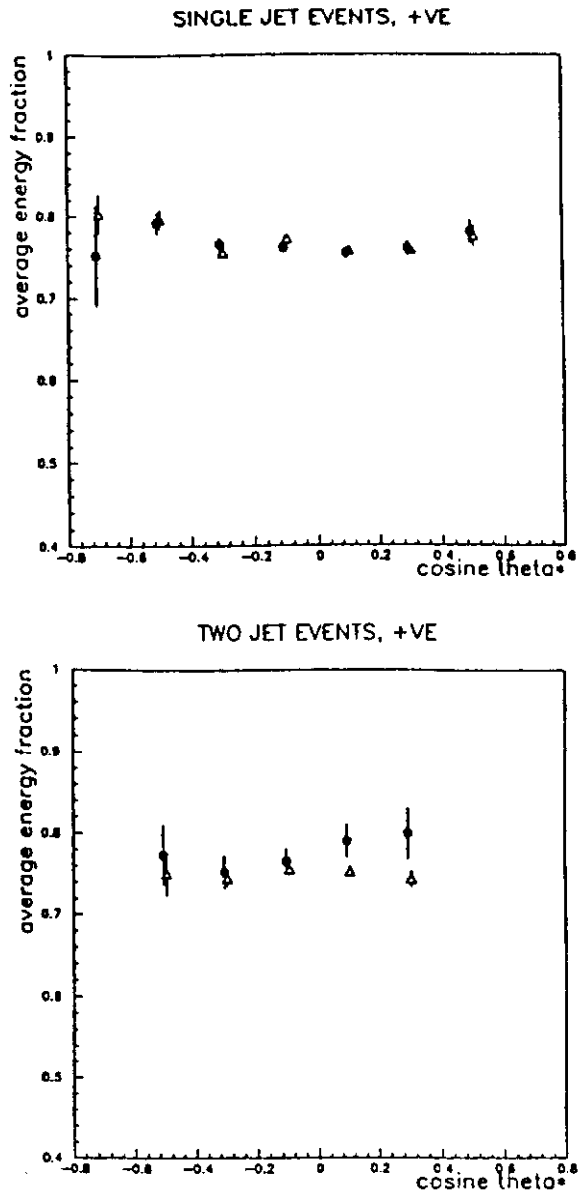

$< \mathcal{Z} >$, function of $\cos\theta^{\star}$ of the leading hadron for single and two jet events and positive leading hadron charge.

- • experimental data
- △ theoretical predictions

Figure 8

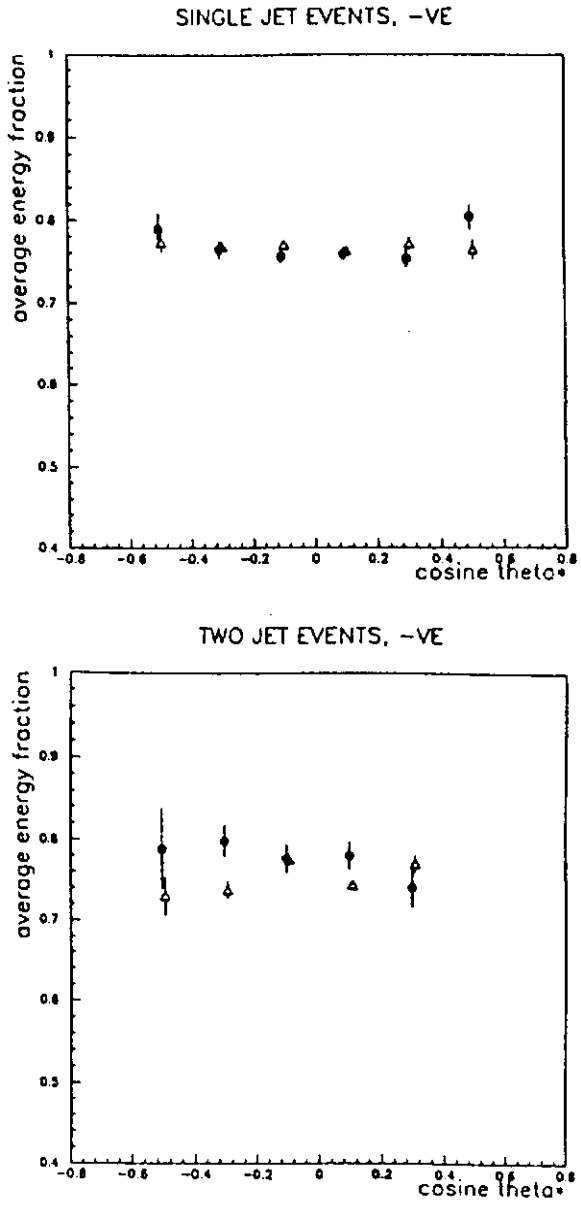

$< \mathcal{Z} >$, function of $\cos\theta^{\star}$ of the leading hadron for single and two jet events and negative leading hadron charge.

- • experimental data
- △ theoretical predictions

Figure 9

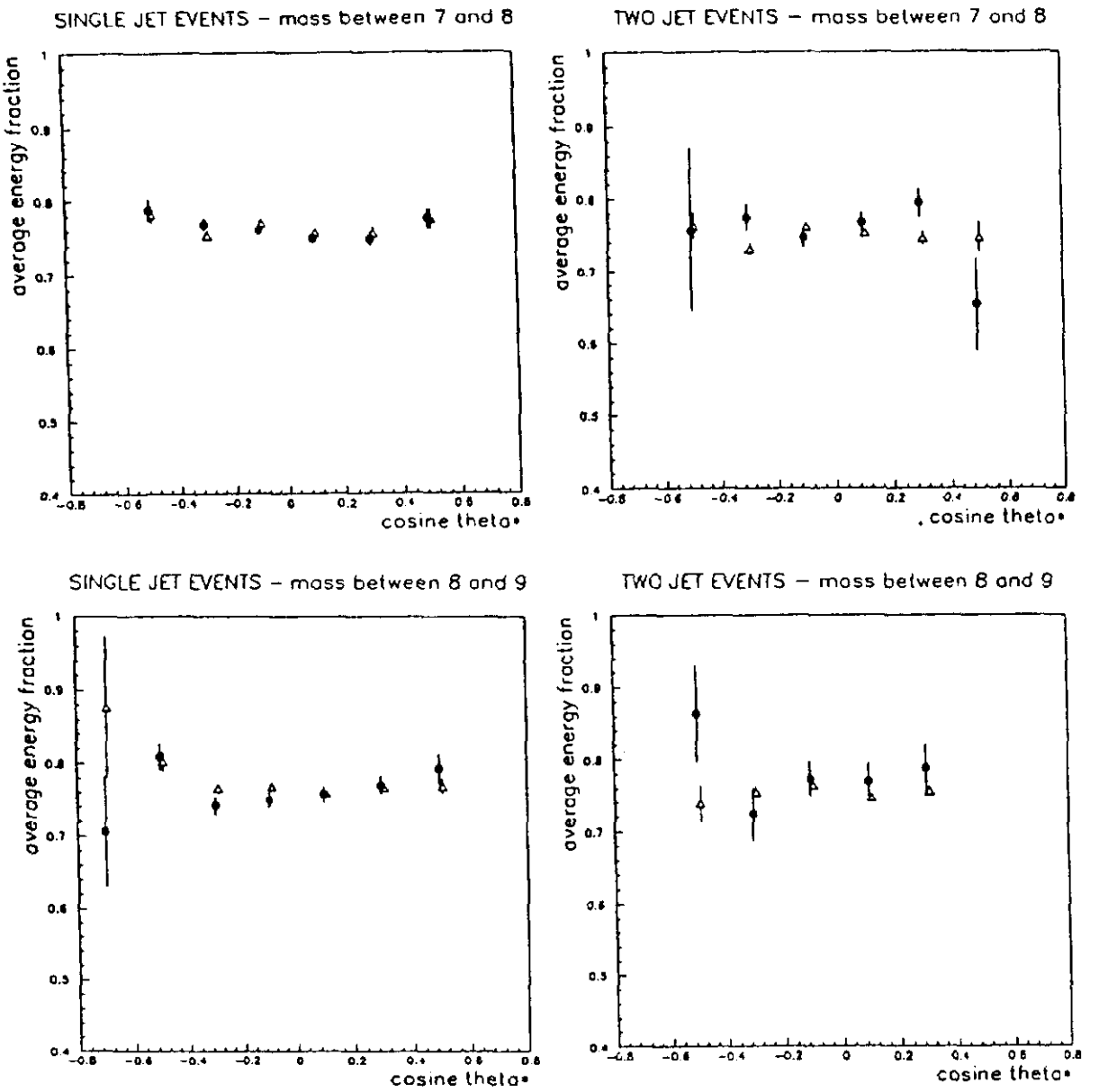

$< z >$, function of $\cos\theta^{\star}$ of the leading hadron for single and two jet events, for different $M_{di-hadron}$ slices and both leading hadron charges.

- • experimental data
- △ theoretical predictions

Figure 10

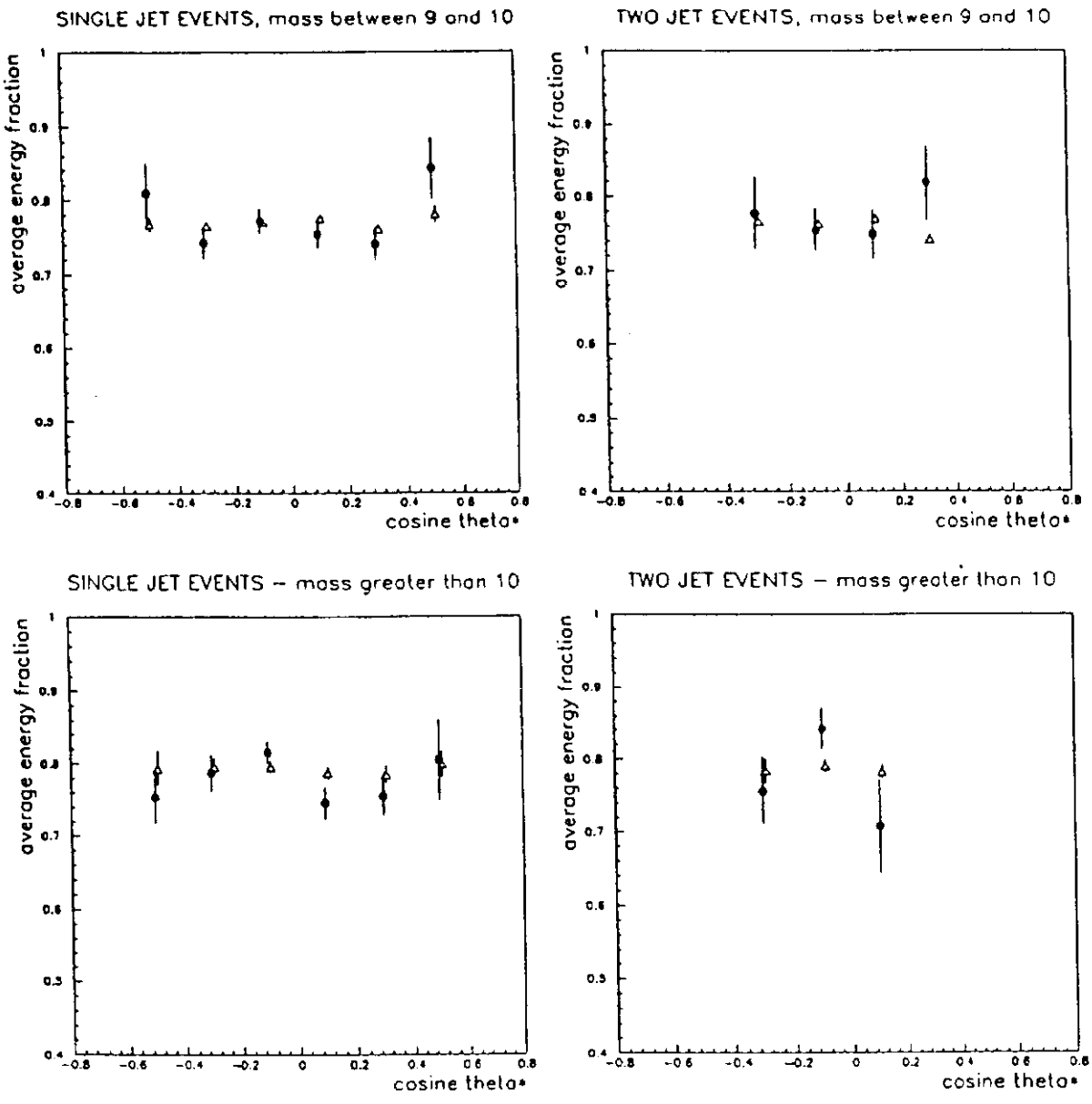

$< \mathcal{Z} >$, function of $\cos\theta^*$ of the leading hadron for single and two jet events, for different $M_{di-hadron}$ slices and both leading hadron charges.

- • experimental data
- △ theoretical predictions

Figure 11

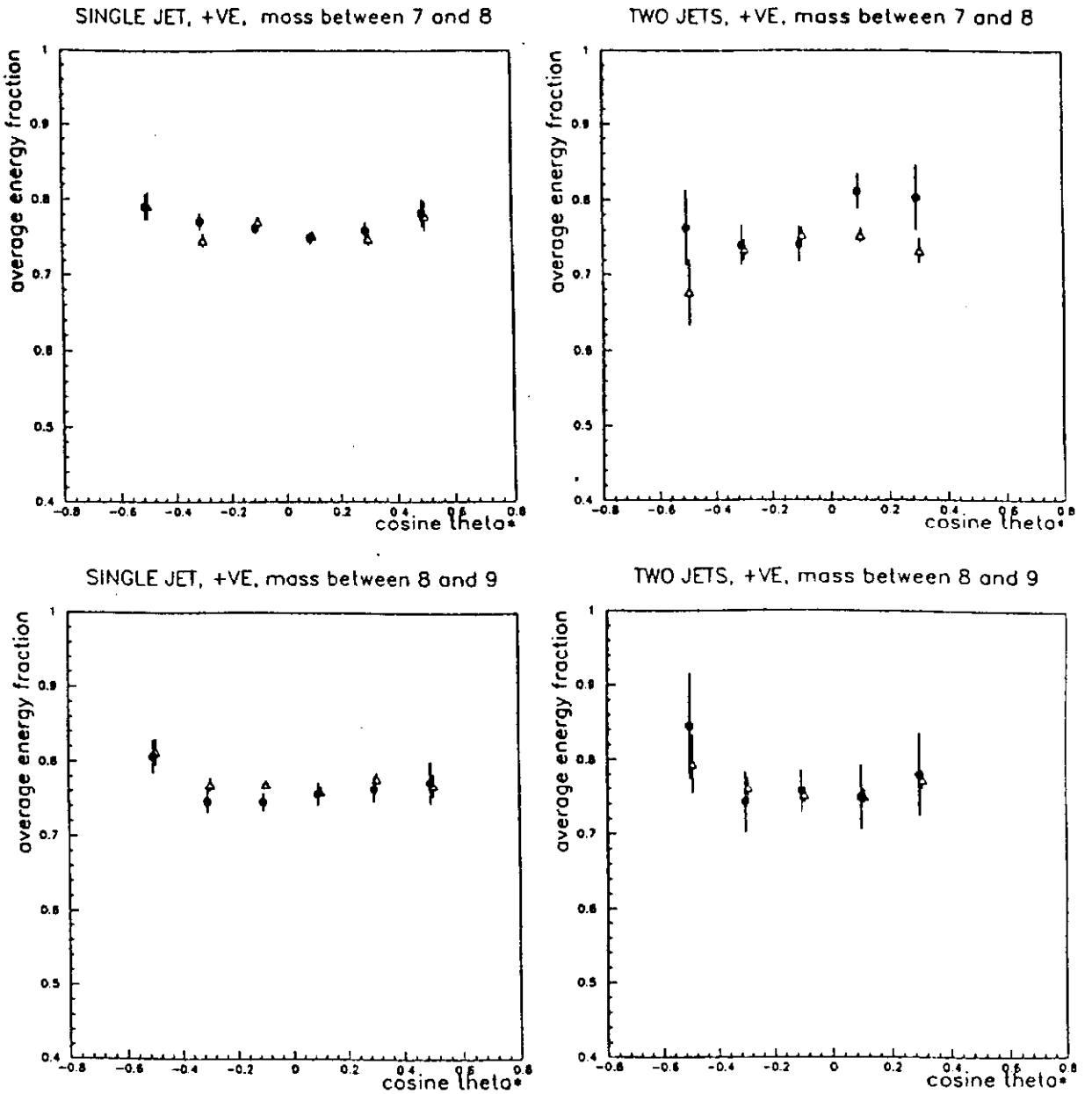

$< \mathcal{Z} >$, function of $\cos\theta^{\star}$ of the leading hadron for single and two jet events, for different $M_{di-hadron}$ slices and positive leading hadron charge.

- • experimental data
- △ theoretical predictions

Figure 12

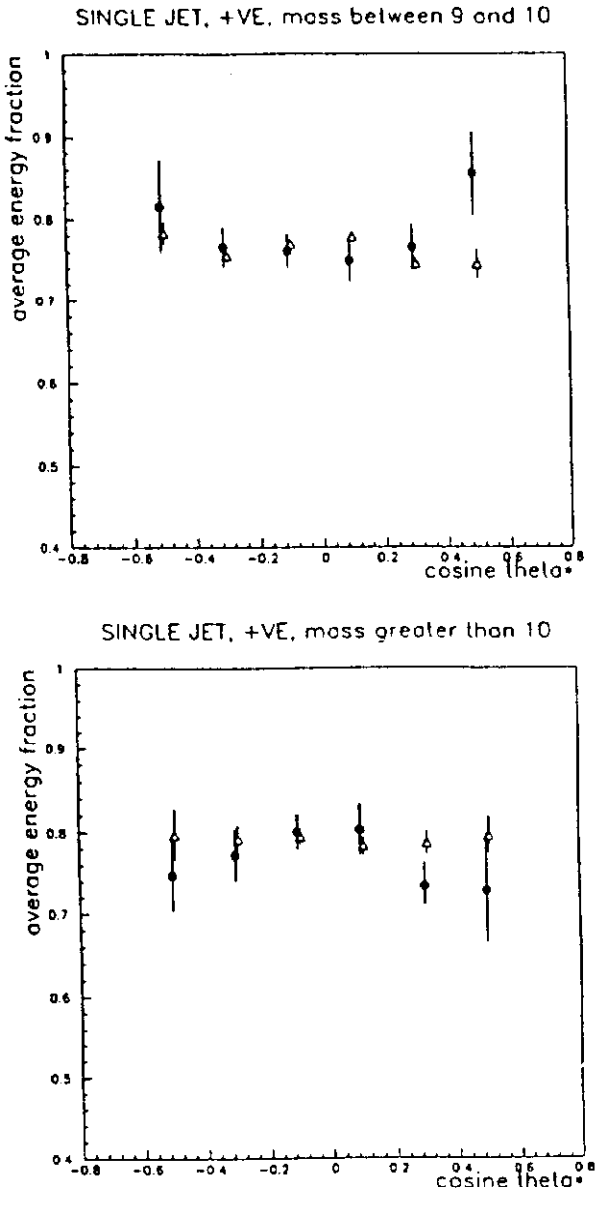

$< z >$, function of $\cos\theta^*$ of the leading hadron for single and two jet events, for different $M_{di-hadron}$ slices and positive leading hadron charge.

- • experimental data
- △ theoretical predictions

Figure 13

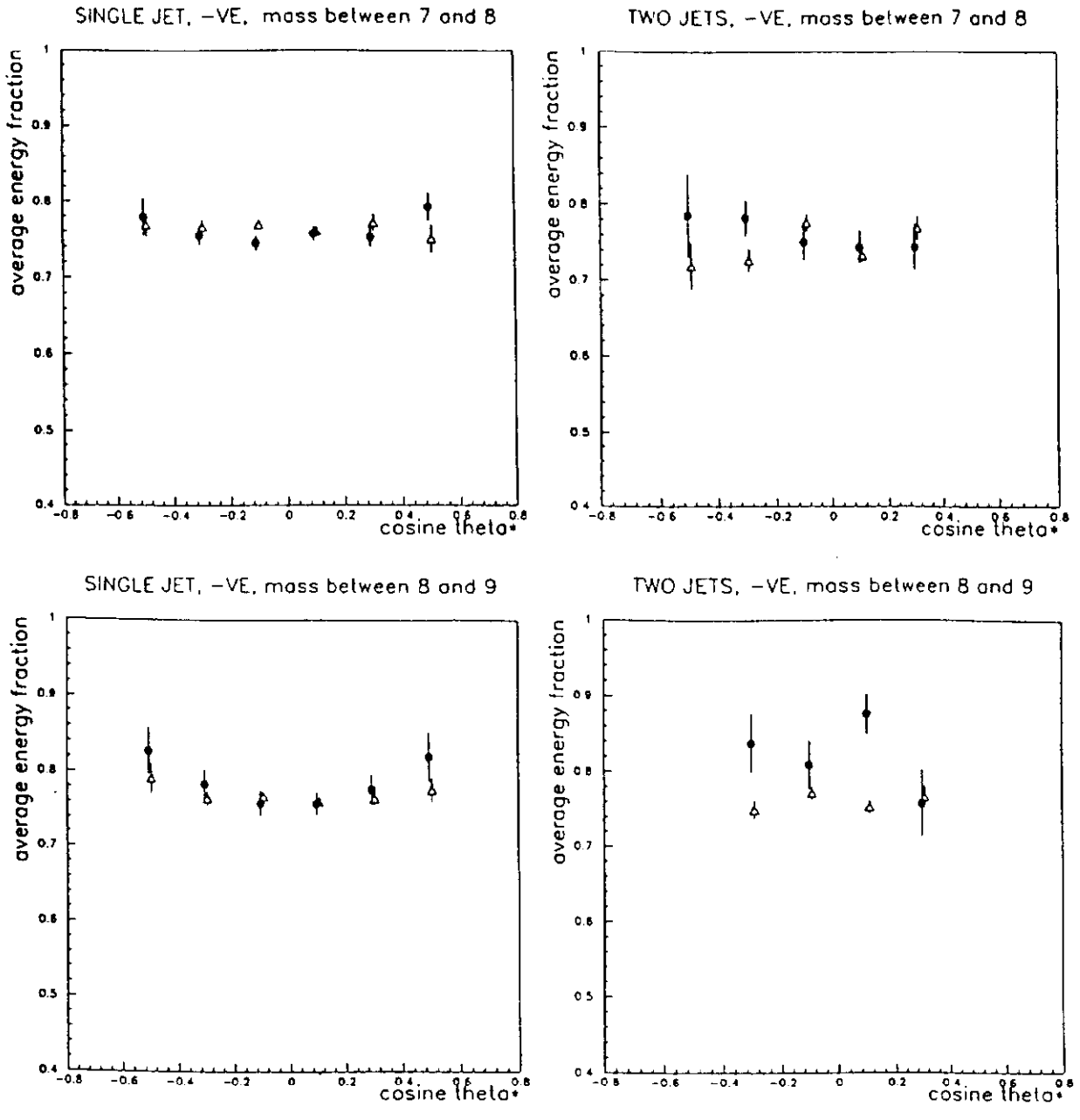

$< \mathcal{Z} >$, function of $\cos\theta^*$ of the leading hadron for single and two jet events, for different $M_{di-hadron}$ slices and negative leading hadron charge.

- • experimental data
- △ theoretical predictions

Figure 14

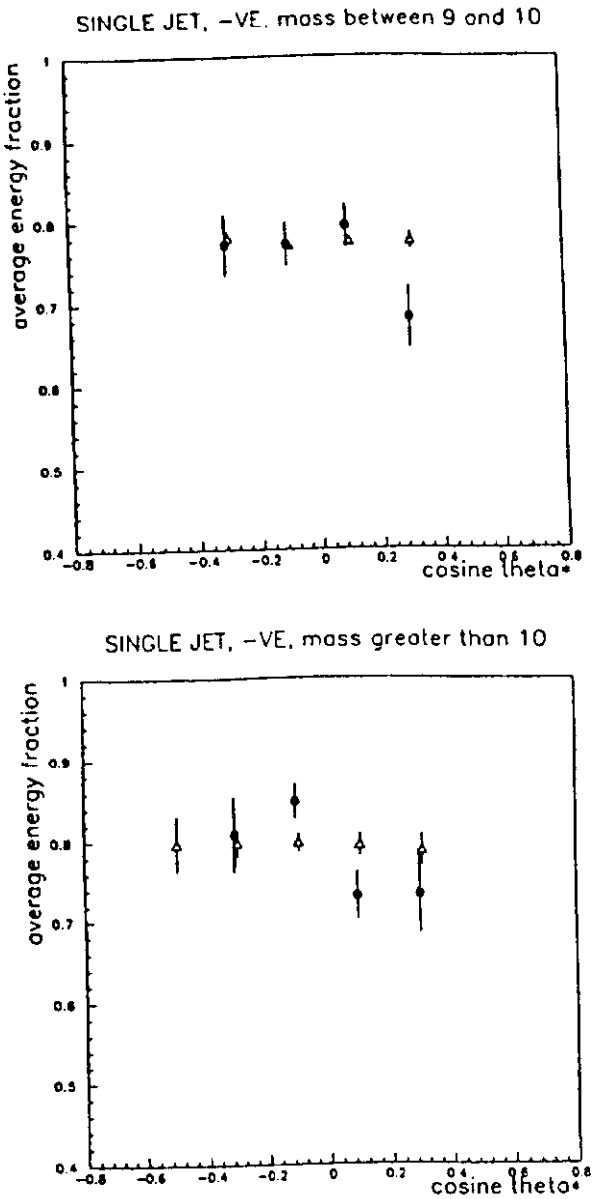

$< Z >$, function of $\cos\theta^{\star}$ of the leading hadron for single and two jet events, for different $M_{di-hadron}$ slices and negative leading hadron charge.

- • experimental data
- △ theoretical predictions

Figure 15